



Hydro-climatic variability in the southwestern Indian Ocean between 6000 and 3000 years ago

Hanying Li¹, Hai Cheng^{1,2}, Ashish Sinha³, Gayatri Kathayat¹, Christoph Spötl⁴, Aurèle Anquetil André⁵, Arnaud Meunier⁵, Jayant Biswas⁶, Pengzhen Duan¹, Youfeng Ning¹, and Richard Lawrence Edwards²

¹Institute of Global Environmental Change, Xi'an Jiaotong University, Xi'an, China

²Department of Earth Sciences, University of Minnesota, Minneapolis, USA

³Department of Earth Science, California State University Dominguez Hills, Carson, USA

⁴Institute of Geology, University of Innsbruck, Innsbruck, Austria

⁵Francois Leguat Giant Tortoise and Cave Reserve, Anse Quitor, Rodrigues Island, Mauritius

⁶National Cave Research and Protection Organization, Raipur, India

Correspondence: Hai Cheng (cheng021@xjtu.edu.cn)

Received: 14 August 2018 – Discussion started: 27 August 2018

Revised: 21 November 2018 – Accepted: 25 November 2018 – Published: 7 December 2018

Abstract. The “4.2 ka event” is frequently described as a major global climate anomaly between 4.2 and 3.9 ka, which defines the beginning of the current Meghalayan age in the Holocene epoch. The “event” has been disproportionately reported from proxy records from the Northern Hemisphere, but its climatic manifestation remains much less clear in the Southern Hemisphere. Here, we present highly resolved and chronologically well-constrained speleothem oxygen and carbon isotopes records between ~ 6 and 3 ka from Rodrigues Island in the southwestern subtropical Indian Ocean, located ~ 600 km east of Mauritius. Our records show that the 4.2 ka event did not manifest itself as a period of major climate change at Rodrigues Island in the context of our record's length. Instead, we find evidence for a multi-centennial drought that occurred near-continuously between 3.9 and 3.5 ka and temporally coincided with climate change throughout the Southern Hemisphere.

1 Introduction

The “4.2 ka event” is considered to be a widespread climate event between 4.2 and 3.9 ka (thousand years before present, where the present is 1950 CE) (e.g. Weiss et al., 1993, 2016). Many paleoclimate records from the Northern Hemisphere (NH) have characterised the event as a multi-decadal to multi-centennial period of arid and cooler conditions across

the Mediterranean, Middle East, South Asia and North Africa (e.g. Finné et al., 2011; Marchant and Hooghiemstra, 2004; Migowski et al., 2006; Mayewski et al., 2004; Staubwasser et al., 2003; Arz et al., 2006; Zielhofer et al., 2017; Stanley et al., 2003; Kathayat et al., 2017). The structure of the 4.2 ka event from many proxy records, such as peat cellulose records from the eastern Tibetan Plateau (Hong et al., 2003, 2018), speleothem from northeastern India (Berkelhammer et al., 2012) and southern Italy (Drysedale et al., 2006), marine sediments from the Gulf of Oman (Cullen et al., 2000) and the northern Red Sea (Arz et al., 2006), and the dust record in the Kilimanjaro ice core (Thompson et al., 2002), typically characterised it as a single pulse-like signal in the long-term context of these records. In contrast, the structure of the 4.2 ka event in the Southern Hemisphere (SH) remains unclear. Some proxy records from the tropical and subtropical regions of Africa and Australia show a shift towards drier conditions around 4 ka (e.g. Russell et al., 2003; Marchant and Hooghiemstra, 2004; Griffiths et al., 2009; Denniston et al., 2013; Berke et al., 2012; De Boer et al., 2013, 2014, 2015; Schefuß et al., 2011; Rijdsdijk et al., 2009, 2011). Other records show virtually unchanged hydrological conditions (e.g. Tierney et al., 2008, 2011; Konecky et al., 2011) or two-pulsed multi-decadal length wet events (Raisback et al., 2018) during the period contemporaneous with the 4.2 ka event.

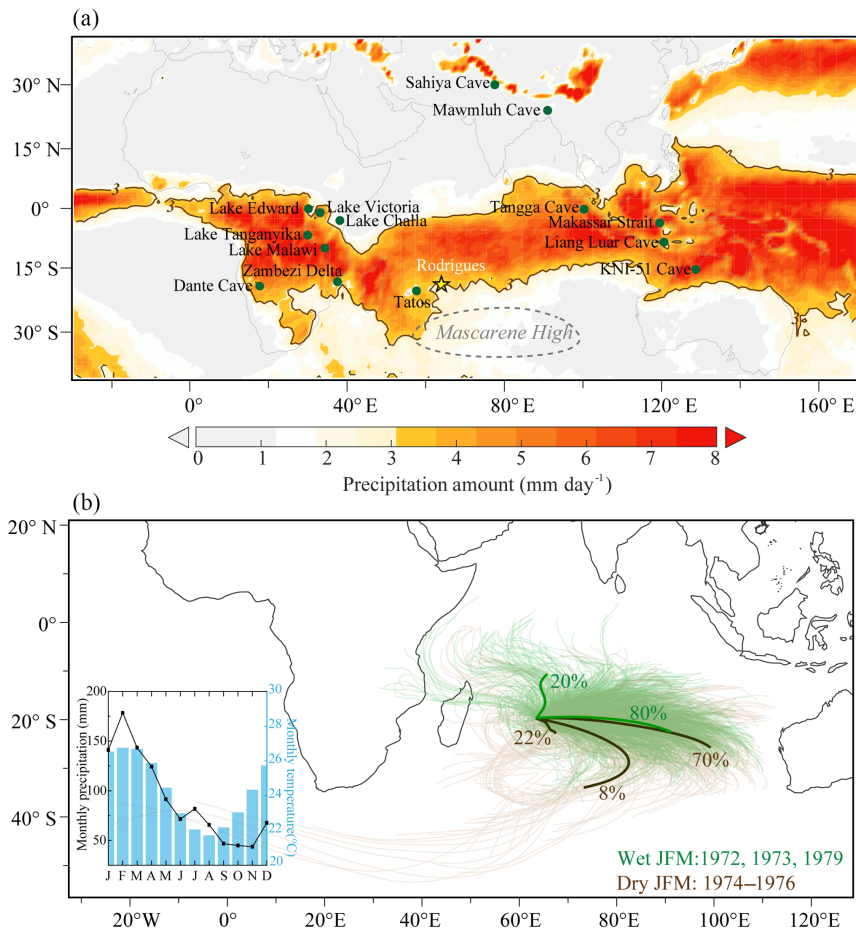


Figure 1. Proxy locations and climatology. **(a)** Mean January to March (JFM) precipitation from the Tropical Rainfall Measuring Mission (TRMM) (<https://trmm.gsfc.nasa.gov/>, last access: 2 December 2018) averaged over the period from 1998 to 2014. The shaded area bounded by solid brown lines (3 mm day^{-1} isohyet) depicts the mean position of the ITCZ. The dashed line shows the mean position of JFM 850 hPa geopotential height marking the location of the Mascarene High. The locations of Rodrigues Island (yellow star, this study) and other proxy sites (green dots) discussed in the text are also shown. **(b)** Four times daily, low-level ($\sim 850 \text{ hPa}$) JFM air parcel back-trajectory (120 h) composites for anomalously wet (green) and dry (brown) years. Trajectories were computed using the NOAA HYSPLIT model (Draxler and Hess, 1998) using NCEP/NCAR reanalysis data (Kalnay et al., 1996). Bold lines indicate main cluster tracks associated with trajectories for wetter (green) and drier (brown) years. Inset shows mean monthly rainfall and temperature at Rodrigues averaged over the period of 1951 to 2015.

The goal of this study is to investigate a time period that spans the 4.2 ka event in a key region of the SH via highly resolved and precisely dated proxy records. Here, we present speleothem oxygen ($\delta^{18}\text{O}$) and carbon ($\delta^{13}\text{C}$) isotope records from La Vierge (LAVI-4) and Patate (PATA-1) caves from the Rodrigues Island (Fig. 1) in the southern subtropical Indian Ocean. The LAVI-4 and PATA-1 records span from ~ 6 to 3 ka and from ~ 6.1 to 3.3 ka, with an average resolution of ~ 4 and 14 years, respectively. LAVI-4, which constitutes our primary record, has a precise age control and a sub-decadal resolution, which, together with the PATA-1 record, allows us to reliably characterise the multi-decadal to centennial hydro-climate variations in the southwestern Indian Ocean during the period from 6 to 3 ka.

2 Modern climatology

2.1 Climatology

Rodrigues ($\sim 19^{\circ}42' \text{ S}$, $\sim 63^{\circ}24' \text{ E}$) is a small volcanic island ($\sim 120 \text{ km}^2$) situated in the southwestern Indian Ocean, $\sim 600 \text{ km}$ east of Mauritius (Fig. 1). The island's maximum altitude is $\sim 400 \text{ m}$ above sea level. Rodrigues' mean annual temperature is $\sim 24^{\circ}\text{C}$ and the mean annual rainfall is $\sim 1010 \text{ mm}$, of which nearly 70% occurs during the wet season (November–April) with February being the wettest month. The seasonal distribution of rainfall is largely controlled by the seasonal migration of the ITCZ (Intertropical Convergence Zone) and the Mascarene High (Senapathi et al., 2010; Rijdsdijk et al., 2011; Morioka et al., 2015) (Fig. 1).

Given its location at the southern fringe of the ITCZ, the austral summer rainfall at Rodrigues is very sensitive to the mean position of the southern limit of the ITCZ. This is highlighted by backward (120 h) HYSPLIT (Draxler and Hess, 1998) trajectory composites of the low-level winds (850 hPa) during the years when the total January to March (JFM) precipitation was unusually low (dry) and high (wet) than the long-term mean (1951–2016) at Rodrigues (Fig. 1b). It is of note that there is a major increase in the fraction of air parcel trajectories arriving from the north of Rodrigues during the wetter years, indicating an enhanced contribution of northerly moisture resulting from a more southerly position of the ITCZ (Fig. 1b). This observation is further supported by analyses of the low-level wind trajectory cluster composites of February in those years when the southern boundary of the ITCZ was anomalously north or south (Lashkari et al., 2017; Freitas et al., 2017) of its long-term mean February position (Fig. S1a, b in the Supplement). In addition to the ITCZ, ENSO (El Niño–Southern Oscillation) also modulates austral summer precipitation at Rodrigues by modulating the Hadley and Walker circulations (Senapathi et al., 2010; De Boer et al., 2014; Griffiths et al., 2016; Zinke et al., 2016). Instrumental data and our trajectory composites for selected El Niño and La Niña years suggest that an increased (decreased) summer precipitation at Rodrigues is associated with the El Niño (La Niña) events (Fig. S1c, d).

2.2 Oxygen isotopes and climatology

Modern observations of $\delta^{18}\text{O}$ of precipitation ($\delta^{18}\text{O}_p$) in the study area are unavailable due to the lack of Global Network of Isotopes in Precipitation (GNIP) stations in Rodrigues. However, $\delta^{18}\text{O}_p$ data from the nearest GNIP station in Mauritius show a clear annual cycle in $\delta^{18}\text{O}_p$ with depleted values during the austral summer (Fig. S2a). Additionally, in the absence of GNIP data, we use simulated $\delta^{18}\text{O}_p$ data from the Experimental Climate Prediction Center's Isotope-incorporated Global Spectral Model (IsoGSM) (Yoshimura et al., 2008) to assess the large-scale dynamical processes that control $\delta^{18}\text{O}_p$ on interannual and decadal timescales. Our analyses show the presence of a strong negative correlation between the $\delta^{18}\text{O}_p$ and rainfall amount similar to the “amount effect” (e.g. Dansgaard, 1964) (Fig. S2b, c). We therefore interpret $\delta^{18}\text{O}_p$ variations in the cave catchment and, consequently, in speleothems from this region as primarily reflecting variations in rainfall amount in response to both local and large-scale atmospheric circulation changes. The relationship is such that more negative (positive) $\delta^{18}\text{O}_p$ values occur during times of either an anomalously southward (northward) position of the southern boundary of the ITCZ or El Niño (La Niña) conditions.

3 Methods

3.1 Speleothem samples

Two stalagmites, LAVI-4 and PATA-1, from La Vierge and Patate caves, respectively, were used in this study. La Vierge ($19^\circ 45' 26''$ S, $63^\circ 22' 13''$ E; ~ 32 m a.s.l.) and Patate ($19^\circ 45' 30''$ S, $63^\circ 23' 11''$ E; ~ 20 m a.s.l.) caves are located in Plaine Corail and Plaine Caverne, respectively, in southwestern Rodrigues (Middleton and David, 2013). The cave temperature and relative humidity at the time of sample collection (June 2015) were $\sim 25.5^\circ\text{C}$ and 95 % in La Vierge Cave and $\sim 22.5^\circ\text{C}$ and 95 % in Patate Cave. Samples LAVI-4 and PATA-1 were collected at a distance of ~ 50 and 200 m from cave entrances, respectively. The diameters of LAVI-4 and PATA-1 are ~ 75 and 95 mm, and their lengths are ~ 400 and ~ 334 mm, respectively. Both stalagmites were cut along their growth axes using a thin diamond blade and then polished.

3.2 ^{230}Th dating

Subsamples (80–130 mg) for ^{230}Th dating were drilled using a 0.9 mm carbide dental drill. ^{230}Th dating was performed at Xi'an Jiaotong University, China, by using a Thermo-Finnigan Neptune Plus, which is a multi-collector inductively coupled plasma mass spectrometer (MC-ICP-MS). The method is described in Cheng et al. (2000, 2013). We used standard chemistry procedures (Edwards et al., 1987) to separate U and Th. A triple-spike (^{229}Tm – ^{233}U – ^{236}U) isotope dilution method was used to correct instrumental fractionation and to determine U/Th isotopic ratios and concentrations (Cheng et al., 2000, 2013). U and Th isotopes were measured on a MasCom multiplier behind the retarding potential quadrupole in the peak-jumping mode using standard procedures (Cheng et al., 2000). Uncertainties in U and Th isotopic measurements were calculated offline at the 2σ level, including corrections for blanks, multiplier dark noise, abundance sensitivity and contents of the same nuclides in the spike solution. ^{234}U and ^{230}Th decay constants of Cheng et al. (2013) were used. Corrected ^{230}Th ages assume an initial $^{230}\text{Th}/^{232}\text{Th}$ atomic ratio of $(4.4 \pm 2.2) \times 10^{-6}$ and those are the values for a material at secular equilibrium with the bulk earth $^{232}\text{Th}/^{238}\text{U}$ value of 3.8. The correction for a few samples in LAVI-4 and PATA-1 is large because either U concentration is low (~ 65 ppb) and/or the detrital ^{232}Th concentration is elevated (> 100 ppt) (Table S1, Fig. 2).

3.3 Stable isotope analysis

LAVI-4 and PATA-1 stable isotope ($\delta^{18}\text{O}$ and $\delta^{13}\text{C}$) records were established by ~ 962 and ~ 190 data, respectively. The New Wave Micromill – digitally controlled tri-axial micromill equipment – was used to obtain subsamples. The subsamples (~ 80 μg) were continuously micro-milled along the stalagmite growth axes of LAVI-4 and PATA-1 at increments

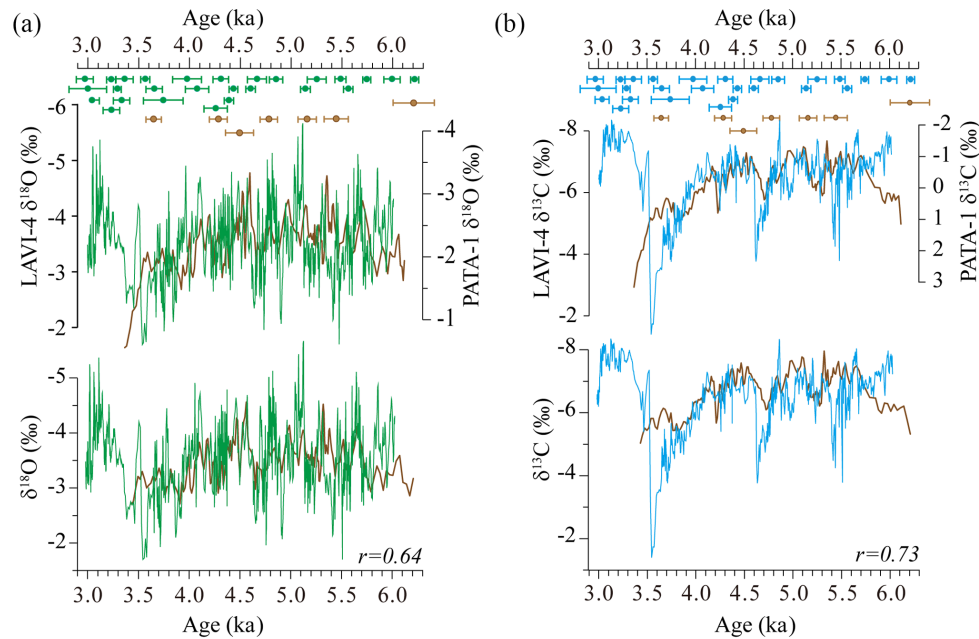


Figure 2. $\delta^{18}\text{O}$ and $\delta^{13}\text{C}$ records of LAVI-4 and PATA-1. **(a)** $\delta^{18}\text{O}$ profiles of LAVI-4 (green) and PATA-1 (brown) are shown on their independent COPRA age models (top diagram) and ISCAM-derived age models (bottom diagram). The correlation coefficient (r) between LAVI-4 and PATA-1 is 0.64. The PATA-1 $\delta^{18}\text{O}$ values were adjusted by $\sim 1.3\text{‰}$ to match the LAVI-4 data series. **(b)** Same as in **(a)** but for the $\delta^{13}\text{C}$ profiles of LAVI-4 and PATA-1. The PATA-1 $\delta^{13}\text{C}$ values were adjusted by $\sim 6.5\text{‰}$ to match the LAVI-4 values.

of between 100 and 200 μm . The subsamples of LAVI-4 were measured using a Finnigan MAT-253 mass spectrometer coupled with an online carbonate preparation system (Kiel-IV) in the Isotope Laboratory, Xi'an Jiaotong University. The subsamples of PATA-1 were measured using an online carbonate preparation system (GasbenchII) connected to an isotope ratio mass spectrometer (Delta^{plus}XL) in the Isotope Laboratory, Innsbruck University. The latter technique is reported in Spötl (2011) and Spötl and Vennemann (2003). All results are reported in per mil (‰) relative to the Vienna PeeDee Belemnite (VPDB) standard. Duplicate measurements of standards show a long-term reproducibility of $\sim 0.1\text{‰}$ (1σ) or better (Table S2, Fig. 2).

4 Results

4.1 Age models

We obtained 26 and 7 ^{230}Th dates for samples LAVI-4 and PATA-1, respectively. The LAVI-4 and PATA-1 age models and associated uncertainties were constructed using the COPRA (Constructing Proxy Records from Age) (Breitenbach et al., 2012) and ISCAM (Intra-Site Correlation Age Modelling) (Fohlmeister, 2012) age modelling schemes (Fig. S3). Both schemes yielded virtually identical age models, and thus the conclusions of this study are not sensitive to the choice of the age model (Figs. 2 and S3).

The time interval from 6 to 3 ka in LAVI-4 speleothem corresponds to a sample depth of 274 to 81 mm below the top, respectively. A drip-water relocation occurred at a depth of 124 mm, which is associated with a Type L surface characterised by slow growth and narrow layers under progressively drier conditions (Railsback et al., 2013) (Figs. S3 and S4). It cannot be ruled out that there is also a hiatus at this depth (~ 3.5 ka). If such a hiatus was indeed present, its duration would be about 100 years based on the age model (Fig. S4). The time interval from 6.1 to 3.3 ka in PATA-1 corresponds to a sample depth of 34 to 15 mm. The growth of PATA-1 ceased at ~ 15 mm and then resumed about 630 years later, creating a hiatus (Fig. S3). The COPRA age models of PATA-1 and LAVI-4 (Figs. 2 and S3) are reported in Table S2 and used in the following discussion.

4.2 Isotopic equilibrium tests

Conventional criteria to assess the isotopic equilibrium of stalagmites are provided by the HENDY Test (Hendy, 1971), which requires no correlation between $\delta^{18}\text{O}$ and $\delta^{13}\text{C}$ values measured along the growth axis as well as along the same growth lamina. The correlation between the $\delta^{18}\text{O}$ and $\delta^{13}\text{C}$ values in LAVI-4 and PATA-1 is 0.53 and 0.85, respectively, which suggests the possibility of isotopic disequilibrium during calcite precipitation. However, a number of studies (e.g. Dorale and Liu, 2009) pointed out that a correlation between $\delta^{18}\text{O}$ and $\delta^{13}\text{C}$ values does not automati-

cally rule out isotopic equilibrium. Instead, the replication test (i.e. a high degree of coherence between $\delta^{18}\text{O}$ profiles of individual speleothems from the same cave) is a more rigorous and reliable test of isotopic equilibrium. Particularly, the replication test is far more robust if the records used are from different caves with different kinetic/vadose-zone processes, as is the case for this study. Indeed, a high degree of visual similarity between the coeval portions of LAVI-4 and PATA-1 $\delta^{18}\text{O}$ and $\delta^{13}\text{C}$ records suggests that both stalagmites record primary climate signals, notwithstanding the offsets between the absolute values (Fig. 2a). The replication is further confirmed by statistically significant correlations between the LAVI-4 and PATA-1 $\delta^{18}\text{O}$ ($r = 0.64$ at 95 % confidence level) and $\delta^{13}\text{C}$ ($r = 0.73$ at 95 % confidence level) records calculated using the ISCAM algorithm (Fohlmeister, 2012) for their contemporary growth period between 3.4 and 6.0 ka (Fig. 2). ISCAM uses a Monte Carlo approach to find the best correlation between the proxy records by adjusting each record within its dating uncertainty. The significant levels are assessed against a red-noise background generated using artificially simulated first-order autoregressive time series (AR1). The offset in absolute $\delta^{18}\text{O}$ values between LAVI-4 and PATA-1, however, remains unclear and possibly arises from processes related to the characteristics of the two karst systems, such as temperature differences as observed during our fieldwork in 2015. Therefore, in the following discussion we focus only on temporal variations of LAVI-4 $\delta^{18}\text{O}$ and $\delta^{13}\text{C}$ records due to their higher resolution and better-constrained chronology (Fig. 2).

5 Discussion and conclusions

5.1 Proxy interpretation

The temporal resolution of the LAVI-4 $\delta^{18}\text{O}$ record between 6 and 3 ka varies from 1.2 to 16.4 years with an average resolution of ~ 3.2 years. The $\delta^{18}\text{O}$ temporal variability is large ($\sim 3.5\text{‰}$) and, as noted earlier, we interpret the $\delta^{18}\text{O}$ variations to dominantly reflect changes in the precipitation amount. This line of reasoning is justified given the island's isolated setting far removed from large-sized landmasses and its low topographic relief, which minimises isotopic variability stemming from processes such as the continentality and altitude effects as well as the mixing of distant water vapour sources with significantly different isotopic compositions. This interpretation is additionally supported by moderate to strong covariance between the LAVI-4 $\delta^{18}\text{O}$ and $\delta^{13}\text{C}$ profiles. Although the process of stalagmite precipitation may be affected by evaporation and/or degassing (Treble et al., 2017; Cuthbert et al., 2014; Markowska et al., 2016; McDermott, 2004; Lachniet, 2009), the temporal variations in the latter can stem from changes in vegetation type and density, soil microbial productivity, prior calcite precipitation (PCP), and groundwater infiltration rates (e.g. Baker et al., 1997; Genty et al., 2003), all of which may drive $\delta^{18}\text{O}$ and $\delta^{13}\text{C}$ values

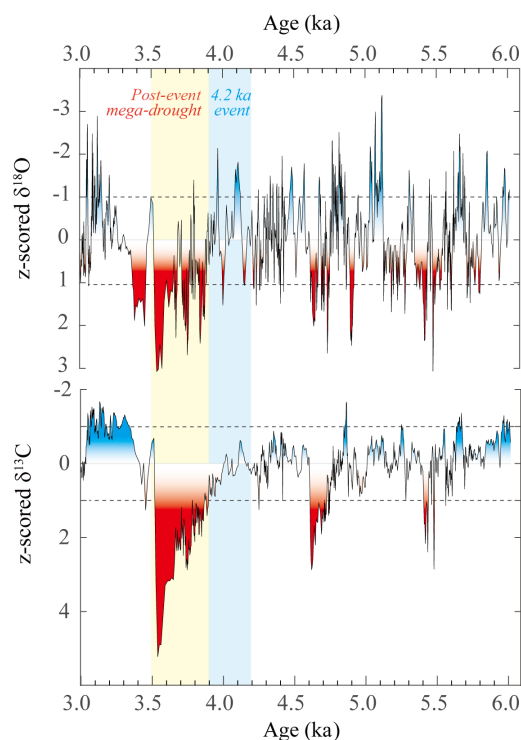


Figure 3. Inferred hydro-climatic variability at Rodrigues from 6 to 3 ka. LAVI-4 $\delta^{18}\text{O}$ and $\delta^{13}\text{C}$ record are z-score transformed. Inferred droughts ($z\text{-score} > 1$) and pluvial episodes ($z\text{-score} < -1$) are shaded (increasing saturation index indicates increasing intensity). Dashed lines indicate 1 standard deviation. The blue bar marks the classical 4.2 ka event interval and the yellow bar marks the “post-event” mega-drought, inferred from LAVI-4.

in the same fashion (e.g. Brook et al., 1990; Dorale et al., 1992; Bar-Matthews et al., 1997). The significant covariance between the $\delta^{13}\text{C}$ and $\delta^{18}\text{O}$ records could therefore indicate that both proxies reflect a common response to changes in rainfall amount at Rodrigues or a rainfall limit on the extent of vegetation and other related processes in the epikarst as mentioned above.

5.2 Hydro-climate variability between 6 and 3 ka at Rodrigues

The z-score-transformed profiles of LAVI-4 $\delta^{18}\text{O}$ and $\delta^{13}\text{C}$ records reveal several decadal to multi-decadal intervals of significantly drier and wetter conditions ($> \pm 1$ standard deviation) (Fig. 3) but no distinct long-term trends (Figs. 2 and 3). The interval corresponding to the 4.2 ka event in the LAVI-4 $\delta^{18}\text{O}$ record, typically between 4.2 and 3.9 ka (e.g. Weiss et al., 2016), includes two dry (~ 4200 to 4130 yr BP and ~ 4020 to 3975 yr BP) and two wet (~ 4130 to 4020 yr BP and ~ 3975 to 3945 yr BP) periods (Fig. 3). During this time interval the LAVI-4 $\delta^{13}\text{C}$ record shows two wet periods peaking at ~ 4115 and 4015 yr BP, respec-

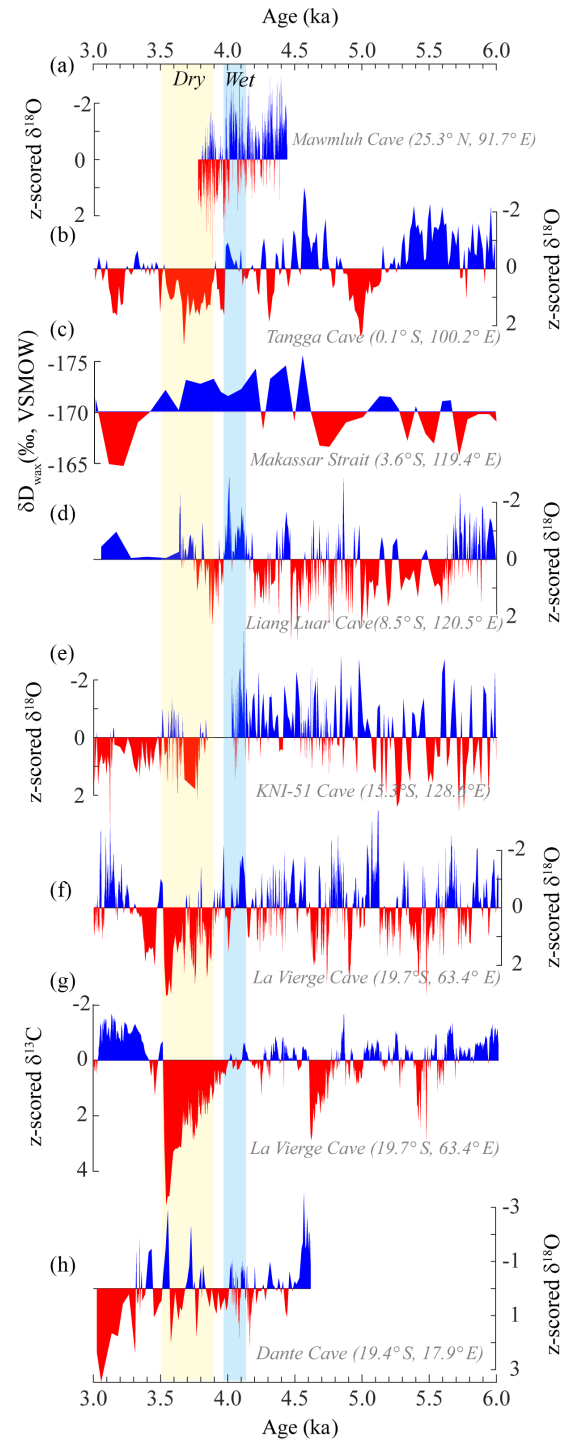


Figure 4. Comparison of LAVI-4 with climate proxy records from the eastern Indian Ocean. From top to bottom, z-score-transformed speleothem $\delta^{18}\text{O}$ record from Mawmluh Cave (Kathayat et al., 2018), Tangga Cave, Sumatra (Indonesia; Wurtzel et al., 2018), $\delta\text{D}_{\text{leaf wax}}$ record from marine sediment core BJ8-03-70GGC in the Makassar Strait (Tierney et al., 2012), z-score-transformed speleothem $\delta^{18}\text{O}$ records from Liang Luar Cave (western Flores, Indonesia; Griffiths et al., 2009), KNI-51 Cave (Kimberley, northwestern Australia; Denniston et al., 2013), La Vierge Cave (Rodrigues; this study) and Dante Cave (northeastern Namibia; Railsback et al., 2018). Shaded vertical bars mark periods of drier and wetter conditions.

tively, which correlate within age uncertainties with two wet pulses in proxy records from Mawmluh Cave (Kathayat et al., 2018), Tangga Cave (Wurtzel et al., 2018), Makassar Strait (Tierney et al., 2012), Liang Luar Cave (Griffiths et al., 2009), KNI-51 Cave (Denniston et al., 2013) and Dante Cave (Railsback et al., 2018) (Fig. 4).

Overall, the climate variations recorded at Rodrigues from 4.2 to 3.9 ka are characterised by high-frequency (decadal to multi-decadal) fluctuations, including the major arid/wet events mentioned above. Notably, however, the mean hydro-climatic state of this time interval inferred from both $\delta^{18}\text{O}$ and $\delta^{13}\text{C}$ data is indistinguishable from the average state between 6 and 4.2 ka (Fig. 3). In this regard, the climatic events or anomalies between 4.2 and 3.9 ka are not distinctly larger in amplitude nor longer in duration in comparison to similar anomalies between 6 and 4.2 ka (Figs. 3 and 4). Consistently, in the context of the long-term climate variance between 6 and 3 ka, there is no evidence for an unusual climate anomaly between 4.2 and 3.9 ka.

The most prominent feature of our record is a switch from an interval characterised by high-frequency $\delta^{18}\text{O}$ variance (i.e. from 6 to 3.9 ka) to a multi-centennial excursion with progressively higher $\delta^{18}\text{O}$ and $\delta^{13}\text{C}$ values: a prolonged mega-drought at Rodrigues. Starting at ~ 3.9 ka, this mega-drought became progressively more severe leading to a diminished growth rate or a ~ 100 yr long hiatus around 3.5 ka in LAVI-4. Growth rate picked up subsequently, followed by abrupt (~ 100 yr long) and large decreases in both $\delta^{18}\text{O}$ ($\sim 2\text{‰}$) and $\delta^{13}\text{C}$ ($\sim 5\text{‰}$) to their average values of the entire records between 6 and 3 ka. As such, the structure of the mega-drought event shows a saw-tooth pattern with a multi-centennial drying trend followed by a ~ 100 yr long return to the mean state (Fig. 3). The multi-century mega-drought recorded by our stalagmites between 3.9 and 3.5 ka is also evident in Sahiya Cave, north India (Kathayat et al., 2017), and from Lake Edward (Russell et al., 2003), Lake Victoria (Berke et al., 2012), the Zambezi Delta (Schefuß et al., 2011) and the Tatos Basin (De Boer et al., 2014) (Fig. 5). In the eastern sector of the southern Indian Ocean, speleothem records from Tangga (Wurtzel et al., 2018), KNI-51 (Denniston et al., 2013) and Liang Luar (Griffiths et al., 2009) caves also show a shift to drier condition at approximately 4 ka (Fig. 4).

The LAVI-4 $\delta^{13}\text{C}$ record shows a pattern broadly similar to the $\delta^{18}\text{O}$ record and clearly delineates three major droughts between 6 and 3 ka, centred at 5.43, 4.62 and 3.54 ka, respectively. These three drought events share a distinct saw-tooth pattern characterised by a long-term gradual positive excursion (drying) followed by an abrupt return to the mean values (Fig. 3).

To sum up, our Rodrigues records show evidence of multi-decadal–decadal hydro-climate fluctuations around the mean state between 6 and 3 ka. After 3.9 ka, the hydro-climate was characterised by a multi-centennial trend toward much drier conditions, which ended with a return at ~ 3.5 ka within \sim

100 years to the mean hydro-climate state. This pattern is different from the “pulse-like” event between 4.2 and 3.9 ka as documented in many other proxy records mainly from the NH. Additionally, the mega-drought between 3.9 and 3.5 ka is clearly a later event unrelated to the 4.2 ka event.

5.3 Possible mechanisms

A close examination of our Rodrigues $\delta^{18}\text{O}$ and $\delta^{13}\text{C}$ records shows that a persistent multi-centennial drying trend began effectively at ~ 4.1 ka and ended at ~ 3.5 ka, suggesting a prolonged northward shift of the mean position of the ITCZ (Figs. 3 and S1a). This inference, if correct, is partially in contrast with the southward shift of the ITCZ, which is often invoked to explain the weakening of the Asian monsoon since ~ 4.2 ka (e.g. Wang et al., 2005; Kathayat et al., 2017). Thus, the observed drying trends on both the northern and southern fringes of the ITCZ in both hemispheres argue against the model of a southward shift in the mean position of the ITCZ as a viable cause of the 4.2 ka event. A more likely explanation involves an overall contraction in the north–south range of the migrating ITCZ belt in the region (e.g. Yan et al., 2015; Denniston et al., 2016; Scroxton et al., 2017). This mechanism is broadly consistent with the spatial pattern of hydro-climate changes observed in both hemispheres around and after the 4.2 ka event. As mentioned above, the wet period between ~ 4.1 and 4.0 ka recorded at the northern fringe of the ITCZ (Kathayat et al., 2017, 2018) coincided with a wet period on the southern limit of the ITCZ as recorded in Dante Cave (Railsback et al., 2018), the Zambezi Delta (Schefuß et al., 2011), Tatos Basin (De Boer et al., 2014), La Vierge Cave (this study) and KNI-51 Cave (Denniston et al., 2013) (Figs. 4 and 5). The subsequent arid period between ~ 3.9 and 3.5 ka was also basin-wide and affected both the northern and southern limits of the ITCZ over the Indian Ocean and adjacent regions (Figs. 4 and 5).

In parallel with drier condition along the southern limit of the austral summer ITCZ, proxy records from Lake Edward (Russell et al., 2003), Lake Victoria (Berke et al., 2012) and Tangga Cave (Wurtzel et al., 2018), which are located near the northern limit of the contemporary austral summer ITCZ, also exhibit drier conditions. In contrast, records within the core location of the austral summer ITCZ, such as Lake Challa (Tierney et al., 2011), Lake Tanganyika (Tierney et al., 2008), Lake Malawi (Konecky et al., 2011) and Makassar Strait (Tierney et al., 2012), show either slightly wetter or virtually unchanged hydro-climatic conditions (Figs. 4 and 5). Based on the observed spatial patterns, we suggest that the contraction of the ITCZ both in terms of a north–south meridional shift as well as with respect to its overall width may have played an important role in modulating the hydro-climate in our study area during and after the 4.2 ka event.

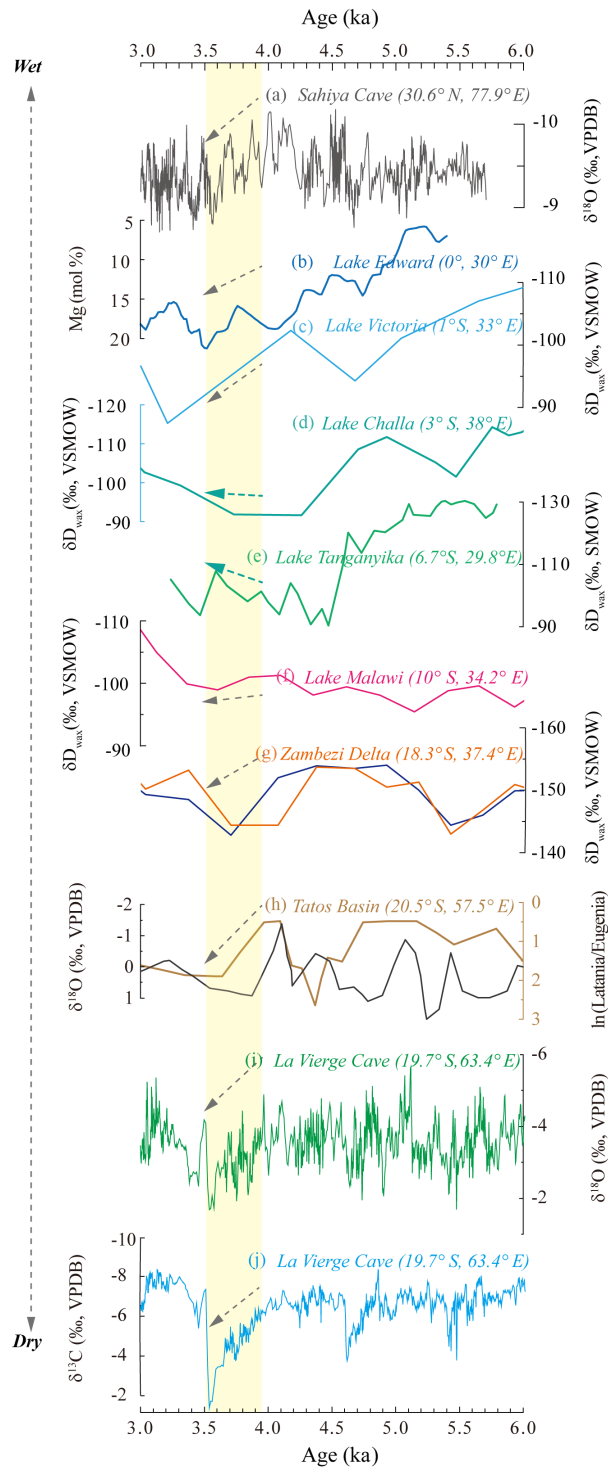


Figure 5. Comparison of LAVI-4 with climate proxy records from India and east Africa. From top to bottom: $\delta^{18}\text{O}$ record from Sahiya Cave (North India; Kathayat et al., 2017), Mg concentration of endogenic calcite from Lake Edward (Russell et al., 2003), $\delta\text{D}_{\text{leaf wax}}$ records from Lake Victoria (Berke et al., 2012), Lake Challa (Tierney et al., 2011), Lake Tanganyika (Tierney et al., 2008), Lake Malawi (Konecky et al., 2011), δD of n-C₂₉ alkanes (dark blue) and n-C₃₁ alkanes (orange) from the Zambezi delta (Scheffuß et al., 2011), $\delta^{18}\text{O}$ record (black) and ln(Latania/Eugenia) records (brown) from Tatos Basin (Mauritius; De Boer et al., 2014), and the LAVI-4 $\delta^{18}\text{O}$ and $\delta^{13}\text{C}$ record from La Vierge Cave (this study). The shaded vertical bar marks the mega-drought from ~ 3.9 to 3.5 ka. Grey and green dashed arrows mark the drying and wet trend inferred from east Africa lake records, respectively. All y axes are inverted to show drier conditions downwards.

Data availability. All data needed to evaluate the conclusions in the paper are presented in the paper. Additional data related to this paper may be requested from the authors. The data will be archived at the National Climate Data Center (<https://www.ncdc.noaa.gov/data-access/paleoclimatology-data>, last access: 2 December 2018). Correspondence and requests for materials should be addressed to Hai Cheng (cheng021@xjtu.edu.cn).

Supplement. The supplement related to this article is available online at: <https://doi.org/10.5194/cp-14-1881-2018-supplement>.

Author contributions. HC, AS and HYL designed the research and experiments; HC, AS, JB, YFN, AAA, AM and HYL completed the fieldwork; HYL, HC, YFN and CS performed stable isotope measurements and ^{230}Th dating work. AS and HYL did the data analyses. HC, HYL and AS wrote the paper, with the help of all co-authors.

Competing interests. The authors declare that they have no conflict of interest.

Special issue statement. This article is part of the special issue “The 4.2 ka BP climatic event”. It is a result of “The 4.2 ka BP Event: An International Workshop”, Pisa, Italy, 10–12 January 2018.

Acknowledgements. We thank Nick Scropton and another anonymous reviewer for their contribution to the peer review of this work. We very much appreciate editorial help from Raymond Bradley. This work was supported by grants from the NSFC (41472140, 41731174 and 41561144003), US NSF grant 1702816 and a grant from the State Key Laboratory of Loess and Quaternary Geology, Institute of Earth Environment, CAS (SKLLQG1414).

Edited by: Raymond Bradley

Reviewed by: Nick Scropton and one anonymous referee

References

- Arz, H. W., Lamy, F., and Pätzold, J.: A pronounced dry event recorded around 4.2 ka in brine sediments from the northern Red Sea, *Quaternary Res.*, 66, 432–441, 2006.
- Baker, A., Ito, E., Smart, P. L., and McEwan, R. F.: Elevated and variable values of ^{13}C in speleothems in a British cave system, *Chem. Geol.*, 136, 263–270, 1997.
- Bar-Matthews, M., Ayalon, A., and Kaufman, A.: Late Quaternary paleoclimate in the eastern Mediterranean region from stable isotope analysis of speleothems at Soreq Cave, Israel, *Quaternary Res.*, 47, 155–168, 1997.
- Berke, M. A., Johnson, T. C., Werne, J. P., Grice, K., Schouten, S., and Damsté, J. S. S.: Molecular records of climate variability and vegetation response since the Late Pleistocene in the Lake Victoria basin, East Africa, *Quaternary Sci. Rev.*, 55, 59–74, 2012.
- Berkelhammer, M., Sinha, A., Stott, L., Cheng, H., Pausata, F. S. R., and Yoshimura, K.: An abrupt shift in the Indian monsoon 4000 years ago, *Geophysical Monograph Series*, 198 pp., 2012.
- Breitenbach, S. F. M., Rehfeld, K., Goswami, B., Baldini, J. U. L., Ridley, H. E., Kennett, D. J., Prufer, K. M., Aquino, V. V., Asmerom, Y., Polyak, V. J., Cheng, H., Kurths, J., and Marwan, N.: COConstructing Proxy Records from Age models (CO-PRA), *Clim. Past*, 8, 1765–1779, <https://doi.org/10.5194/cp-8-1765-2012>, 2012.
- Brook, G. A., Burney, D. A., and Cowart, J. B.: Desert paleoenvironmental data from cave speleothems with examples from the Chihuahuan, Somali-Chalbi, and Kalahari deserts, *Palaeogeogr. Palaeoclimatol.*, 76, 311–329, 1990.
- Cheng, H., Edwards, R., Hoff, J., Gallup, C., Richards, D., and Asmerom, Y.: The half-lives of uranium-234 and thorium-230, *Chem. Geol.*, 169, 17–33, 2000.
- Cheng, H., Edwards, R. L., Shen, C.-C., Polyak, V. J., Asmerom, Y., Woodhead, J., Hellstrom, J., Wang, Y., Kong, X., and Spötl, C.: Improvements in ^{230}Th dating, ^{230}Th and ^{234}U half-life values, and U–Th isotopic measurements by multi-collector inductively coupled plasma mass spectrometry, *Earth Planet. Sci. Lett.*, 371, 82–91, 2013.
- Cullen, H., DeMenocal, P., Hemming, S., Hemming, G., Brown, F., Guilderson, T. and Sirocko, F.: Climate change and the collapse of the Akkadian empire: Evidence from the deep sea, *Geology*, 28, 379–382, 2000.
- Cuthbert, M. O., Baker, A., Jex, C. N., Graham, P. W., Treble, P. C., Andersen, M. S., and Acworth, R. I.: Drip water isotopes in semi-arid karst: implications for speleothem paleoclimatology, *Earth Planet. Sci. Lett.*, 395, 194–204, 2014.
- Dansgaard, W.: Stable isotopes in precipitation, *Tellus*, 16, 436–468, 1964.
- De Boer, E. J., Hooghiemstra, H., Florens, F. B. V., Baider, C., Engels, S., Dakos, V., Blaauw, M., and Bennett, K. D.: Rapid succession of plant associations on the small ocean island of Mauritius at the onset of the Holocene, *Quaternary Sci. Rev.*, 68, 114–125, 2013.
- De Boer, E. J., Tjallingii, R., Vélez, M. I., Rijdsdijk, K. F., Vlug, A., Reichert, G. J., Prendergast, A. L., Louw, P. G. B. D., Florens, F. B. V., and Baider, C.: Climate variability in the SW Indian Ocean from an 8000-yr long multi-proxy record in the Mauritian lowlands shows a middle to late Holocene shift from negative IOD-state to ENSO-state, *Quaternary Sci. Rev.*, 86, 175–189, 2014.
- De Boer, E. J., Velez, M. I., Rijdsdijk, K. F., Louw, P. G. D., Vernimmen, T. J., Visser, P. M., Tjallingii, R., and Hooghiemstra, H.: A deadly cocktail: How a drought around 4200 cal. yr BP caused mass mortality events at the infamous “dodo swamp” in Mauritius, *Holocene*, 25, 758–771, 2015.
- Denniston, R. F., Wyrwoll, K. H., Polyak, V. J., Brown, J. R., Asmerom, Y., Jr, A. D. W., Lapointe, Z., Ellerbroek, R., Barthelmes, M., and Cleary, D.: A Stalagmite record of Holocene Indonesian–Australian summer monsoon variability from the Australian tropics, *Quaternary Sci. Rev.*, 78, 155–168, 2013.
- Denniston, R. F., Ummenhofer, C. C., Wanamaker, A. D., Lachniet, M. S., Villarini, G., Asmerom, Y., Polyak, V. J., Passaro, K. J., Cugley, J., Woods, D., and Humphreys, W. F.: Expansion and contraction of the Indo-Pacific tropical rain belt over the last three millennia, *Sci. Rep.*, 6, 34485, <https://doi.org/10.1038/srep34485>, 2016.

- Dorale, J. A. and Liu, Z.: Limitations of Hendy test criteria in judging the paleoclimatic suitability of speleothems and the need for replication, *J. Cave Karst Stud.*, 71, 73–80, 2009.
- Dorale, J. A., González, L. A., Reagan, M. K., Pickett, D. A., Murrell, M. T., and Baker, R. G.: A high-resolution record of Holocene climate change in speleothem calcite from Cold Water Cave, northeast Iowa, *Science*, 258, 1626–1630, 1992.
- Draxler, R. R. and Hess, G. D.: An overview of the HYSPLIT_4 modelling system for trajectories, *Aust. Meteorol. Mag.*, 47, 295–308, 1998.
- Drysdale, R., Zanchetta, G., Hellstrom, J., Maas, R., Fallick, A., Pickett, M., Cartwright, I., and Piccini, L.: Late Holocene drought responsible for the collapse of Old World civilizations is recorded in an Italian cave flowstone, *Geology*, 34, 101–104, 2006.
- Edwards, R. L., Chen, J., and Wasserburg, G.: ^{238}U – ^{234}U – ^{230}Th – ^{232}Th systematics and the precise measurement of time over the past 500,000 years, *Earth Planet. Sci. Lett.*, 81, 175–192, 1987.
- Finné, M., Holmgren, K., Sundqvist, H. S., Weiberg, E., and Lindblom, M.: Climate in the eastern Mediterranean, and adjacent regions, during the past 6000 years—A review, *J. Archaeol. Sci.*, 38, 3153–3173, 2011.
- Fohlmeister, J.: A statistical approach to construct composite climate records of dated archives, *Quat. Geochronol.*, 14, 48–56, 2012.
- Freitas, A. C. V., Aímola, L., Ambrizzi, T., and de Oliveira, C. P.: Extreme Intertropical Convergence Zone shifts over Southern Maritime Continent, *Atmos. Sci. Lett.*, 18, 2–10, 2017.
- Genty, D., Blamart, D., Ouahdi, R., Gilmour, M., Baker, A., Jouzel, J., and Van-Exter, S.: Precise dating of Dansgaard–Oeschger climate oscillations in western Europe from stalagmite data, *Nature*, 421, 833–837, 2003.
- Griffiths, M. L., Drysdale, R. N., Gagan, M. K., Zhao, J. X., Ayliffe, L. K., Hellstrom, J. C., Hantoro, W. S., Frisia, S., Feng, Y. X., and Cartwright, I.: Increasing Australian–Indonesian monsoon rainfall linked to early Holocene sea-level rise, *Nat. Geosci.*, 2, 636–639, 2009.
- Griffiths, M. L., Kimbrough, A. K., Gagan, M. K., Drysdale, R. N., Cole, J. E., Johnson, K. R., Zhao, J. X., Cook, B. I., Hellstrom, J. C., and Hantoro, W. S.: Western Pacific hydroclimate linked to global climate variability over the past two millennia, *Nat. Comm.*, 7, 11719, <https://doi.org/10.1038/ncomms11719>, 2016.
- Hendy, C. H.: The isotopic geochemistry of speleothems – I. The calculation of the effects of different modes of formation on the isotopic composition of speleothems and their applicability as palaeoclimatic indicators, *Geochim. Cosmochim. Ac.*, 35, 801–824, 1971.
- Hong, Y. T., Hong, B., Lin, Q. H., Zhu, Y. X., Shibata, Y., Hirota, M., Uchida, M., Leng, X. T., Jiang, H. B., Xu, H., Wang, H., and Yi, L.: Correlation between Indian Ocean summer monsoon and North Atlantic climate during the Holocene, *Earth Planet. Sci. Lett.*, 211, 371–380, 2003.
- Hong, B., Uchida, M., Hong, Y., Peng, H., Kondo, M., and Ding, H.: The respective characteristics of millennial-scale changes of the India summer monsoon in the Holocene and the Last Glacial, *Palaeogeogr. Palaeoclimatol.*, 496, 155–165, 2018.
- Kalnay, E., Kanamitsu, M., Kistler, R., Collins, W., Deaven, D., Gandin, L., Iredell, M., Saha, S., White, G., Woollen, J., Zhu, Y., Chelliah, M., Ebisuzaki, W., Higgins, W., Janowiak, J., Mo, K. C., Ropelewski, C., Wang, J., Leetmaa, A., Reynolds, R., Jenne, R. and Joseph, D.: The NCEP/NCAR 40-year reanalysis project, *B. Am. Meteorol. Soc.*, 77, 437–472, 1996.
- Kathayat, G., Cheng, H., Sinha, A., Yi, L., Li, X., Zhang, H., Li, H., Ning, Y., and Edwards, R. L.: The Indian monsoon variability and civilization changes in the Indian subcontinent, *Sci. Adv.*, 3, e1701296, <https://doi.org/10.1126/sciadv.1701296>, 2017.
- Kathayat, G., Cheng, H., Sinha, A., Berkelhammer, M., Zhang, H., Duan, P., Li, H., Li, X., Ning, Y., and Edwards, R. L.: Evaluating the timing and structure of the 4.2 ka event in the Indian summer monsoon domain from an annually resolved speleothem record from Northeast India, *Clim. Past*, 14, 1869–1879, <https://doi.org/cp-14-1869-2018>, 2018.
- Konecky, B. L., Russell, J. M., Johnson, T. C., Brown, E. T., Berke, M. A., Werne, J. P., and Huang, Y.: Atmospheric circulation patterns during late Pleistocene climate changes at Lake Malawi, Africa, *Earth Planet. Sci. Lett.*, 312, 318–326, 2011.
- Lachniet, M. S.: Climatic and environmental controls on speleothem oxygen-isotope values, *Quaternary Sci. Rev.*, 28, 412–432, 2009.
- Lashkari, H., Mohammadi, Z., and Keikhosravi, G.: Annual Fluctuations and Displacements of Inter Tropical Convergence Zone (ITCZ) within the Range of Atlantic Ocean–India, *Open Journal of Ecology*, 7, 12–33, <https://doi.org/10.4236/oje.2017.71002>, 2017.
- Marchant, R. and Hooghiemstra, H.: Rapid environmental change in African and South American tropics around 4000 years before present: a review, *Earth-Sci. Rev.*, 66, 217–260, 2004.
- Markowska, M., Baker, A., Andersen, M. S., Jex, C. N., Cuthbert, M. O., Rau, G. C., Graham, P. W., Rutledge, H., Mariethoz, G., Marjo, C. E., Treble, P. C., Edwards, N.: Semiarid zone caves: evaporation and hydrological controls on $\delta^{18}\text{O}$ drip water composition and implications for speleothem paleoclimate reconstructions, *Quaternary Sci. Rev.*, 131, 285–301, 2016.
- Mayewski, P. A., Rohling, E. J., Stager, J. C., Karlén, W., Maasch, K. A., Meeker, L. D., Meyerson, E. A., Gasse, F., Van Kreveld, S., Holmgren, K., Lee-Thorp, K., Rosqvist, G., Rack, F., Staubwasser, M., Schneider, R. R., and Steig, E. J.: Holocene climate variability, *Quaternary Res.*, 62, 243–255, 2004.
- McDermott, F.: Palaeo-climate reconstruction from stable isotope variations in speleothems: a review, *Quaternary Sci. Rev.*, 23, 901–918, 2004.
- Middleton, G. J. and David A. B.: Rodrigues – An Indian Ocean Island calcarenite: its history, study and management, *Coastal Karst Landforms*, Springer, Dordrecht, 261–276, 2013.
- Migowski, C., Stein, M., Prasad, S., Negendank, J. F., and Agnon, A.: Holocene climate variability and cultural evolution in the Near East from the Dead Sea sedimentary record, *Quaternary Res.*, 66, 421–431, 2006.
- Morioka, Y., Takaya, K., Behera, S. K., and Masumoto, Y.: Local SST impacts on the summertime Mascarene high variability, *J. Climate*, 28, 678–694, 2015.
- Railsback, L. B., Akers, P. D., Wang, L., Holdridge, G. A., and Voarintsoa, N.: Layer-bounding surfaces in stalagmites as keys to better paleoclimatological histories and chronologies, *Int. J. Speleol.*, 42, 167–180, 2013.
- Railsback, L. B., Liang, F., Brook, G. A., Voarintsoa, N. R. G., Sletten, H. R., Marais, E., Hardt, B., Cheng, H., and Edwards, R. L.: The timing, two-pulsed nature, and variable climatic expression

- of the 4.2 ka event: A review and new high-resolution stalagmite data from Namibia, *Quaternary Sci. Rev.*, 186, 78–90, 2018.
- Rijsdijk, K. F., Hume, J. P., Bunnik, F., Florens, F. B. V., Baider, C., Shapiro, B., Plicht, J. V. D., Janoo, A., Griffiths, O., and Ostende, L. W. V. D. H.: Mid-Holocene vertebrate bone Concentration-Lagerstätte on oceanic island Mauritius provides a window into the ecosystem of the dodo (*Raphus cucullatus*), *Quaternary Sci. Rev.*, 28, 14–24, 2009.
- Rijsdijk, K. F., Zinke, J., Louw, D. P. G. B., Hume, J. P., Plicht, V. D. H., Hooghiemstra, H., Meijer, H. J. M., Vonhof, H. B., Porch, N., and Florens, F. B. V.: Mid-Holocene (4200 yr BP) mass mortalities in Mauritius (Mascarenes): insular vertebrates resilient to climatic extremes but vulnerable to human impact, *Holocene*, 21, 1179–1194, 2011.
- Russell, J. M., Johnson, T. C., and Talbot, M. R.: A 725 yr cycle in the climate of central Africa during the late Holocene, *Geology*, 31, 677–680, 2003.
- Schefuß, E., Kuhlmann, H., Mollenhauer, G., Prange, M., and Pätzold, J.: Forcing of wet phases in southeast Africa over the past 17,000 years, *Nature*, 480, 509–512, <https://doi.org/10.1038/nature10685>, 2011.
- Scroxton, N., Burns, S. J., McGee, D., Hardt, B., Godfrey, L. R., Ranivoharimanana, L., and Faina, P.: Hemispherically in-phase precipitation variability over the last 1700 years in a Madagascar speleothem record, *Quaternary Sci. Rev.*, 164, 25–36, 2017.
- Senapathi, D., Underwood, F., Black, E., Nicoll, M. A., and Norris, K.: Evidence for long-term regional changes in precipitation on the East Coast Mountains in Mauritius, *Int. J. Climatol.*, 30, 1164–1177, 2010.
- Spötl, C.: Long-term performance of the Gasbench isotope ratio mass spectrometry system for the stable isotope analysis of carbonate microsamples, *Rapid Commun. Mass Sp.*, 25, 1683–1685, 2011.
- Spötl, C. and Vennemann, T. W.: Continuous-flow isotope ratio mass spectrometric analysis of carbonate minerals, *Rapid Commun. Mass Sp.*, 17, 1004–1006, 2003.
- Stanley, J.-D., Krom, M. D., Cliff, R. A., and Woodward, J. C.: Short contribution: Nile flow failure at the end of the Old Kingdom, Egypt: strontium isotopic and petrologic evidence, *Geochronology*, 18, 395–402, 2003.
- Staubwasser, M., Sirocko, F., Grootes, P., and Segl, M.: Climate change at the 4.2 ka BP termination of the Indus valley civilization and Holocene south Asian monsoon variability, *Geophys. Res. Lett.*, 30, 1425, <https://doi.org/10.1029/2002GL016822>, 2003.
- Thompson, L. G., Mosley-Thompson, E., Davis, M. E., Henderson, K. A., Brecher, H. H., Zagorodnov, V. S., Mashiotto, T. A., Lin, P., Mikhalenko, V. N., Hardy, D. R., and Beer, J.: Kilimanjaro ice core records: evidence of Holocene climate change in tropical Africa, *Science*, 298, 589–593, 2002.
- Tierney, J. E., Russell, J. M., Huang, Y., Damsté, J. S. S., Hoppmans, E. C., and Cohen, A. S.: Northern Hemisphere controls on tropical southeast African climate during the past 60,000 years, *Science*, 322, 252–255, 2008.
- Tierney, J. E., Russell, J. M., Damsté, J. S. S., Huang, Y., and Verschuren, D.: Late Quaternary behavior of the East African monsoon and the importance of the Congo Air Boundary, *Quaternary Sci. Rev.*, 30, 798–807, 2011.
- Tierney, J. E., Oppo, D. W., LeGrande, A. N., Huang, Y., Rosenthal, Y., and Linsley, B. K.: The influence of Indian Ocean atmospheric circulation on Warm Pool hydroclimate during the Holocene epoch, *J. Geophys. Res.-Atmos.*, 117, D19108, <https://doi.org/10.1029/2012JD018060>, 2012.
- Treble, P. C., Baker, A., Ayliffe, L. K., Cohen, T. J., Hellstrom, J. C., Gagan, M. K., Frisia, S., Drysdale, R. N., Griffiths, A. D., and Borsato, A.: Hydroclimate of the Last Glacial Maximum and deglaciation in southern Australia's arid margin interpreted from speleothem records (23–15 ka), *Clim. Past*, 13, 667–687, <https://doi.org/10.5194/cp-13-667-2017>, 2017.
- Wang, Y., Cheng, H., Edwards, R. L., He, Y., Kong, X., An, Z., Wu, J., Kelly, M. J., Dykoski, C. A., and Li, X.: The Holocene Asian monsoon: links to solar changes and North Atlantic climate, *Science*, 308, 854–857, 2005.
- Weiss, H., Courty, M.-A., Wetterstrom, W., Guichard, F., Senior, L., Meadow, R., and Curnow, A.: The genesis and collapse of third millennium north Mesopotamian civilization, *Science*, 261, 995–1004, 1993.
- Weiss, H.: Global megadrought, societal collapse and resilience at 4.2–3.9 ka BP across the Mediterranean and west Asia, *PAGES*, 24, 62–63, 2016.
- Wurtzel, J. B., Abram, N. J., Lewis, S. C., Bajo, P., Hellstrom, J. C., Troitzsch, U., and Heslop, D.: Tropical Indo-Pacific hydroclimate response to North Atlantic forcing during the last deglaciation as recorded by a speleothem from Sumatra, Indonesia, *Earth Planet. Sci. Lett.*, 492, 264–278, 2018.
- Yan, H., Wei, W., Soon, W., An, Z., Zhou, W., Liu, Z., Wang, Y., and Carter, R. M.: Dynamics of the intertropical convergence zone over the western Pacific during the Little Ice Age, *Nat. Geosci.*, 8, 315–320, 2015.
- Yoshimura, K., Kanamitsu, M., Noone, D., and Oki, T.: Historical isotope simulation using reanalysis atmospheric data, *J. Geophys. Res.-Atmos.*, 113, D19108, <https://doi.org/10.1029/2008JD010074>, 2008.
- Zielhofer, C., Suchodoletz, H. V., Fletcher, W. J., Schneider, B., Dietze, E., Schlegel, M., Schepanski, K., Weninger, B., Mischke, S., and Mikdad, A.: Millennial-scale fluctuations in Saharan dust supply across the decline of the African Humid Period, *Quaternary Sci. Rev.*, 171, 119–135, 2017.
- Zinke, J., Reuning, L., Pfeiffer, M., Wassenburg, J. A., Hardman, E., Jhangeer-Khan, R., Davies, G. R., Ng, C. K. C., and Kroon, D.: A sea surface temperature reconstruction for the southern Indian Ocean trade wind belt from corals in Rodrigues Island (19° S, 63° E), *Biogeosciences*, 13, 5827–5847, <https://doi.org/10.5194/bg-13-5827-2016>, 2016.